Clim. Past Discuss., https://doi.org/10.5194/cp-2018-145
Manuscript under review for journal Clim. Past
Discussion started: 13 November 2018

Mid-Holocene climate change over China: model-data discrepancy

Yating Lin [1,2,4], Gilles Ramstein [2], Haibin Wu [1,3,4], Raj Rani [2], Pascale Braconnot [2], Masa Kageyama [2], Qin Li [1,3], Yunli Luo [5], and Zhengtang Guo [1,3,4]

1. Key Laboratory of Cenozoic Geology and Environment, Institute of Geology and Geophysics, Chinese Academy of Sciences, Beijing 100029, China

2. Laboratoire des Sciences du Climat et de l'Environnement, LSCE/IPSL, CEA-CNRS-UVSQ, Université Paris-Saclay, Gif-sur-Yvette 91191, France

3. CAS Center for Excellence in Life and Paleoenvironment, Beijing, 100044, China

4. University of Chinese Academy of Sciences, Beijing 100049, China

5. Institute of Botany, Chinese Academy of Sciences, Beijing 100093, China

Abstract:

The mid-Holocene period (MH) has long been an ideal target for the validation of Global Circulation Model (GCM) results against proxy reconstructions gathered in global datasets. These studies aimed to test the GCM sensitivity mainly to the seasonal changes induced by the orbital parameters (precession). Despite widespread agreement between model results and data on the MH climate, some important differences still exist. There is no consensus on the continental size of the MH thermal climate response, which makes regional quantitative reconstruction critical to obtain a comprehensive understanding of MH climate patterns. Here, we compare the annual and seasonal outputs from the most recent Paleoclimate Modelling and Coupled Modelling Intercomparison Projects Phase 3 (PMIP3) models with an updated synthesis of temperature reconstruction over China, including, for the first time, a seasonal cycle. Most of the models provide a linear response driven by the seasonal forcing (warmer in summer, cooler in winter), which disagrees with the new seasonal data reconstruction over

China. We show that to capture the seasonal pattern reconstructed by data, it is critical to access surface processes. These results pinpoint the crucial importance of including the non-linear process associated with vegetation changes in hydrology and radiative forcing.

Keywords: PMIP3 Pollen data Inverse Vegetation Model Seasonal climate change

1. Introduction

Much attention of paleoclimate study has been focused on the current interglacial (the Holocene), especially the mid-Holocene (MH, 6±0.5ka). The major difference in the experimental configuration between MH and pre-Industrial (PI) arises from the orbital parameters which brings about an increase in isolation in the seasonal cycle of the Northern Hemisphere and a decrease in the Southern Hemisphere (Berger, 1978). Thus, the MH provides an excellent case study on which to base an evaluation of the climate response to seasonal distributions of insolation. Great efforts are devoted by the modeling community to the design of MH common experiments using similar boundary conditions (Joussaume and Taylor, 1995; Harrison et al., 2002; Braconnot et al., 2007a,b). In addition, much work has been done to constrain the consistency of the dataset incorporating different proxies at global and continental scale (Guiot et al., 1993; Kohfeld and Harrison, 2000; Prentice et al., 2000; Bartlein et al., 2011). The greatest progress in understanding MH climate change and variability has consistently been made by comparing large-scale analyses of proxy data with simulations from global climate models (Joussaume et al., 1999; Liu et al., 2004; Harrison et al., 2014).

Clim. Past Discuss., https://doi.org/10.5194/cp-2018-145
Manuscript under review for journal Clim. Past
Discussion started: 13 November 2018

However, the discrepancies between model and data is still an open and stimulating question. Two types of inconsistencies have been identified: 1) where the model and data show opposite signs, for instance, paleoclimate evidence from data-records indicates an increase of about 0.5K in global annual mean temperature during MH compared with PI (Shakun et al. 2012; Marcott et al. 2013), while there is a cooling trend in model simulations (Liu et al., 2014). 2) where the same trend is displayed by both model and data but with different magnitudes. Previous studies have shown that while climate models can successfully reproduce the direction and large-scale patterns of past climate changes, they tend to consistently underestimate the magnitude of change in the monsoons of the Northern Hemisphere as well as the amount of MH precipitation over northern Africa (Braconnot et al., 2012; Harrison et al., 2015). Moreover, significant spatial variability has been noted in both observations and simulations (Peyron et al. 2000; Davis et al. 2003; Braconnot et al., 2007a; Wu et al. 2007; Bartlein et al. 2011), which makes regional quantitative reconstruction (Davis et al., 2003; Mauri et al., 2015) essential to obtain a comprehensive understanding of MH climate patterns, and to act as a benchmark to evaluate climate models (Fischer and Jungclaus, 2011; Harrison et al., 2014;).

China offers two advantages in respect to these issues. The sheer expanse of the country means that the continental response to insolation changes over a large region can be investigated. Moreover, the quantitative reconstruction of seasonal climate changes during MH, based on the new pollen dataset, provides a unique opportunity to compare the seasonal cycles for models and data. Previous studies indicate that warmer and wetter conditions prevailed over China during MH and that the magnitude of the annual temperature increases varied from 2.4-5.8K spatially, with an annual precipitation increase in the range of 34-267mm (e.g., Sun et al., 1996; Jiang et al., 2010; Lu et al., 2012; Chen et al., 2015). However, Jiang et al. (2012) clearly show a mismatch between multi-proxy reconstructions and model simulations. In terms of climate anomalies (MH-PI), besides the ~1K increase in summer temperature, 35 out of 36

Clim. Past Discuss., https://doi.org/10.5194/cp-2018-145
Manuscript under review for journal Clim. Past
Discussion started: 13 November 2018

Paleoclimate Modelling and Coupled Modelling Intercomparison Projects (PMIP) models reproduce annual (~0.4K) and winter temperatures (~1.4K) that are colder than the baseline, and a drier-than-baseline climate in some western and middle regions over China is depicted in models (Jiang et al. 2013). This study firstly pinpoints the model-data discrepancy over China during MH, but the lack of statistical seasonal reconstruction hampers the quantitative comparison of data with simulations for seasonal climate.

An important issue raised by Liu et al. (2014) is that the discrepancy at the annual level could be due to incorrect reconstructions of the seasonal cycle, a key objective in our paper. Moreover, it has been suggested that the vegetation change can strengthen the temperature response in high latitudes (O'Ishi et al., 2009; Otto et al., 2009), as well as alter the hydrological conditions in the tropics (Liu et al., 2007). However, compared to the substantial land cover changes in MH derived from pollen datasets (Ni et al., 2010; Yu et al., 2000; Bartlein et al., 2011), the changes in vegetation have not yet been fully quantified and discussed in PMIP3 (Tylor et al., 2012).

In this study, for the reconstruction, we firstly used the quantitative method of biomization to reconstruct vegetation types during MH based on a new synthesis of pollen datasets, and then used the process-based biogeographic model—the Inverse Vegetation Model (Guiot et al. 2000; Wu et al. 2007, 2016) to obtain the annual, the mean temperature of the warmest month (MTWA) and the mean temperature of the coldest month (MTCO) climate features over China for the MH. In the case of models, we present a comprehensive evaluation of the state-of-the-art models based on MH climate variables (vegetation, temperature and precipitation), using the simulations from the PMIP3. This is the first time that such progress towards a quantitative seasonal climate comparison for MH over China has been made, thanks to the seasonal reconstruction and the PMIP3 results. This point is crucial because of the fact that the forcing factor we used for MH is essential the seasonal change. We will thus be able to answer the question posed by Liu et al. (2014) on the importance of seasonal reconstruction.

2. Data and Methodology

2.1 Data

In this study, we collected 159 pollen records, covering most of China, for the MH period (6±0.5ka ^{14}C timescale) (Fig. 1). Of these, 65 were from the Chinese Quaternary Pollen Database (CQPD, 2001), 3 were original datasets obtained in our study, and the others were digitized from pollen diagrams in published papers with a recalculation of pollen percentages based on the total number of terrestrial pollen types. These digitized 91 pollen records were selected according to three criteria: (1) distinct pollen diagrams with a reliable chronology with the minimum of three independent age control points since the LGM; (2) a minimum sampling resolution of 1000 years per sample and only extracted the pollen taxa during the 6±0.5ka period; (3) located far from archeological sites to avoid the influence of human activity. The age-depth model for the pollen records was estimated by linear interpolation between adjacent available dates or regression. The quality of dating control for the mid-Holocene was assessed by assigning a rank from 1 to 7, using ranking schemes from the Cooperative Holocene Mapping Project, and 70% of the records fell into the first and second classes (see Table 1 for detailed information) according to the Webb 1-7 standards (Webb, 1985). Vegetation type was quantitatively reconstructed using biomization, following the classification of plant functional types (PFTs) and biome assignment in China by the Members of China Quaternary Pollen Data (CQPD, 2001), which has been widely tested in surface sedimentary. The new sites added to our database improved the spatial coverage of pollen records, especially in the northwest, the

Tibetan Plateau, the Loess Plateau and southern regions, where the data in the previous databases are very limited.

Modern monthly mean climate variables, including temperature, precipitation and cloudiness, have been spatially interpolated for each modern pollen site based on the datasets (1951-2001) from 657 meteorological observation stations over China. A 3-layer back-propagation (BP) artificial neural network technique (ANN) was used for interpolation on each pollen site (Caudill and Butler, 1992). Five input variables (latitude, longitude, elevation, annual precipitation, annual temperature) and one output variable (biome scores) have been chosen in ANN for the modern vegetation. The ANN has been calibrated on the training set, and its performance has been evaluated on the verification set (20%, randomly extracted from the total sets). After a series of training run, the lowest verification error is obtained with 5 neurons in the hidden layer after 10000 iterations. The anomalies between past (6ka) and modern vegetation indices (biome scores) was then interpolated to the 0.2×0.2° grid resolution by applying the ANN. After that, the modern grid values are added to the values of the grid of palaeo-anomalies to provide gridded paleo-biome indices. Finally, the biome with the highest index is attributed to each grid point. This ANN method is more efficient than many other techniques on condition that the results are validated by independent data sets, and therefore, it has been widely applied in paleoclimatology (Guiot et al., 1996; Peyron et al., 1998). Soil properties were derived from the digital world soil map produced by the Food and Agricultural organization (FAO) (FAO, 1995), and, because of a lack of paleosol data, soil characteristics were assumed to have been the same during MH. Atmospheric CO_2 concentration for the MH was taken from ice core records (EPICA community members 2004), and set at 270 ppmv.

2.2 Climate models

PMIP, a long-standing initiative, is a climate-model evaluation project which provides an efficient mechanism for using global climate models to simulate climate anomalies in the present day and to understand the role of climate feedback. In its third phase (PMIP3), the models were identical to those used in the Climate Modelling Intercomparison Project 5 (CMIP5) experiments, in which the PI experiment was defined. The experimental set-up for PMIP3 MH simulations followed the PMIP protocol (Braconnot et al. 2007a, b, 2012). The main variability between MH and PI in PMIP3 are the orbital configuration and CH_4 concentration. More precisely, the orbital configuration in the MH climate has an increased summer insolation and a decreased winter insolation in the Northern Hemisphere compared to the PI climate (Berger, 1978). Meantime, the CH_4 concentration is prescribed at 650 ppbv in MH, while it is set at 760 ppbv in PI (Table 2).

All 13 models (Table 3) from PMIP3 that have MH simulation have been included in our study, including 8 ocean-atmosphere (OA) models and 5 ocean-atmosphere-vegetation (OAV) models. Means for the last 30 years were calculated from the archived time-series data on individual model grids for climate variables: near surface temperature and precipitation flux, which were bi-linearly interpolated to a common 2.5° grid, in order to calculate bioclimatic variables (e.g. MAT, MAP, MTWM, MTCO, July precipitation) for comparison with the reconstruction results.

2.3 Vegetation model

The vegetation model, BIOME4 is a coupled bio-geography and bio-geochemistry model developed by Kaplan et al. (2003). Monthly mean temperature, precipitation, sunshine percentage (relative to cloud cover), absolute minimum temperature, atmospheric CO_2 concentration and subsidiary information about the soil's physical properties like water retention capacity and percolation rates are the main input variables for the models. It incorporates 13 plant functional types (PFTs), which have different bioclimatic limits. The PFTs are based on physiological attributes and bioclimatic tolerance limits such as heat, moisture and chilling requirements and resistance of plants to cold. These limits determine the areas where the PFTs could grow in a given climate. A viable combination of these PFTs defines a particular biome among 28 potential options. These 28 biomes can be further classified into 8 megabiomes (Table S1). BIOME4 has been widely utilized to analyze the past, present and potential future vegetation patterns (e.g. Bigelow et al., 2003; Diffenbaugh et al., 2003; Song et al., 2005). In this study, we conducted 13 PI and MH biome simulations using PIMP3/CMIP5 climate fields (temperature, precipitation and sunshine) as inputs. The climate fields, obtained from PMIP3/CMIP5, are the monthly mean data of more than 30 model years.

2.4 Statistics and interpolation for vegetation distribution

To quantify the model-data disparities between megabiomes, a map-based statistic (point-to-point comparison with observations) called ΔV (Sykes et al., 1999; Ni et al., 2000) was applied to our study. ΔV is based on the relative abundance of different plant life forms (e.g. trees, grass, bare ground) and a series of attributes (e. g. evergreen, needle-leaf, tropical, boreal) for each vegetation class. The definitions and attributes of each plant form follow naturally from the BIOME4 structure and the vegetation attribute values in the ΔV computation were defined for BIOME4 in the same way as for BIOME1 (Sykes et al., 1999). The abundance and attribute values are given in Table 4 and Table 5, which estimate the typical floristic composition of the biomes. Weighting the attributes is subjective because there is no obvious theoretical basis for assigning relative significance. Transitions between highly dissimilar megabiomes have a weighting of close to 1, whereas transitions between less dissimilar megabiomes are assigned smaller values. The overall dissimilarity between model and data megabiome maps was calculated by averaging the ΔV for the grids with pollen data, while the value was set at 0 for any grid without data. ΔV values < 0.15 can be considered to point to very good agreement between simulated and actual distributions, 0.15-0.30 is good, 0.30-0.45 fair, 0.45-0.60 poor, and > 0.80 very poor (adjusted from Zhang et al., 2010). For spatial pattern comparison, we used the back-propagation (BP) artificial neural network technique again for interpolation, as described above for climate variables (see data section), to obtain the spatial pattern of megabiomes from pollen records. Secondly, we compared the simulated vegetation distribution from BIOME4 from each model with the interpolated pattern.

2.5 Inverse vegetation model

A process-based biogeography model, named Inverse Vegetation Model (Guiot et al., 2000; Wu et al. 2007), which is highly dependent on the BIOME4 model, is applied to our reconstruction. The key concept of this model can be summarized in two points: firstly, a set of transfer functions able to transform the model output into values directly comparable with pollen data is defined. There is not full compatibility between the biome typology of BIOME4 and the biome typology of pollen data. A transfer matrix (Table S2) was defined in our study where each BIOME4 vegetation type is assigned a vector of values, one of each pollen vegetation type, ranging from 0 (representing an incompatibility between BIOME4 type and pollen biome type) to 15 (corresponding to a maximum compatibility). Secondly, using an iterative approach, a representative set of climate scenarios compatible with the vegetation records is identified among the climate space, constructed by systematically perturbing the input variables (e.g. atmospheric CO_2 concentration, soil, ΔT, ΔP) of the model (Table S3).

Inverse Vegetation Model (IVM) provides a possibility, for the first time, to reconstruct both annual and seasonal climates for MH over China. Moreover, it offers a way to consider the impact of CO_2 concentration on competition between PFTs as well as on the relative abundance of taxa, and thus make reconstruction from pollen records more reliable. More detailed information about IVM can be found in Wu et al. (2007).

We applied the inverse model to modern pollen samples to validate the approach by reconstructing the modern climate at each site and comparing it with the observed values. The high correlation coefficients (R=0.75–0.95), intercepts close to 0 (except for the mean temperature of the warmest month), and slopes close to 1 (except for the July precipitation) demonstrated that the inversion method worked well for most variables in China (see Table 6).

3. Results

3.1 Comparison of annual and seasonal climate changes at MH

In this study, we collected 159 pollen records, broadly covering the whole of China (Fig. 1). To check the reliability of the collected data, we first categorized our pollen records into megabiomes in line with the standard tables developed for the BIOME6000 (Table S1), and compared them with the BIOME6000 dataset (Fig.2). The match between collected data and the BIOME6000 is more than 90% for both MH and PI.

Based on pollen records, the spatial pattern of climate changes over China during MH, deduced from IVM, are presented in Fig. 3 (left panel, points), alongside the results from PMIP3 models (shaded in Fig. 3). For temperature, a warmer-than-present annual climate condition (~0.7K on average) is derived from pollen data (the points in Fig. 3a), with the largest increase occurring in the northeast (3-5K) and a decrease in the northwest and on Tibetan Plateau. On the other hand, the results from a multi-model ensemble (MME) indicate a colder annual temperature generally (~-0.4K on average), with significant cooling in the south and slight warming in the northeast (shaded in Fig. 3a). Of the 13 models, 11 simulate a cooler annual temperature compared with PI as MME. However, two models (HadeGEM2-ES and CNRM-CM5) present the same warmer trend as was found in the reconstruction (Fig. 3d). Compared to the reconstruction, the annual mean temperature during MH is largely underestimated by most PMIP3 models, which depict an anomaly ranging from ~-1.4 to ~0.5 K. Detailed information of reconstructed climate change derived from IVM at each pollen site can be found in Table S4.

Concerning seasonal change, during MH, MTWA from the data is ~0.5 K higher than PI, with the largest increase in the northeast and a decrease in the northwest. From model outputs, an average increase of ~1.2 K is reproduced by MME, with a more pronounced warming at high latitudes which is consistent with the insolation change (Berger, 1978). Fig. 3e shows that all 13 models reproduce the same warmer summer temperatures as the data, and that HadGEM2-ES and CNRM-CM5, reproduce the largest increases among the models. Although the warmer MTWA is consistent between the models and data, there is a discrepancy between them on MTCO. In Fig. 3c, the data show an overall increase of ~1 K, with the largest increase occurring in the northeast and a decrease of opposite magnitude on the Tibetan Plateau. Inversely, MME reproduces a decreasing trend with an average amplitude of ~-1.3 K, the coolest areas being the southeast, the Loess Plateau and the northwest. Similarly to the MME, all 13 models simulate a colder-than-present climate with amplitudes ranging from ~-2.0 K (CCSM4 and FGOALS-g2) to ~-0.7 K (HadGEM2-ES and CNRM-CM5).

Concerning annual change in precipitation, the reconstruction shows wetter conditions during MH across almost the whole of China with the exception of part of the northwest. The southeast presents the largest increase in annual precipitation. All but 2 models depict wetter conditions with an amplitude of ~10mm to ~70mm. The reconstruction and MME results also indicate an increasing trend (Fig.4a), with a much larger magnitude visible in the reconstruction (~30mm, ~230mm respectively). The main discrepancy in annual precipitation between simulations and reconstruction occurs in the northeast, which is depicted as drier by the models and wetter by the data. With regard to seasonal change, the reconstruction shows an overall increase in July rainfall (~50mm on average), with a decrease in the northwestern regions. In line with the reconstruction, the MME also shows an overall increase in rainfall (~13mm on average), with a decrease in the northwest for July (Fig.4b). Notably, a much larger increase is simulated for the south and the Tibetan Plateau by the models, while the opposite pattern emerges along the eastern margin from both models and data. More detailed information about the geographic distribution of temperature and precipitation for each model can be found in Fig. S1-S6.

3.2 Comparison of vegetation change at MH

The use of the PMIP3 database is clearly limited by the different vegetation inputs among the models for the MH period. Only HadGEM2-ES and HadGEM2-CC use a dynamic vegetation for MH, and the other 11 models are prescribed to PI with or without interactive LAI, which would introduce a bias to the role of vegetation-atmosphere interaction in MH climates. To evaluate the model results against the reconstruction for MH vegetation, we conducted 13 biome simulations in BIOME4 using PIMP3 climate fields, and the megabiome distribution for each model during MH is displayed in Fig. 5 (see Fig. S7 for PI vegetation comparison). To quantify the model-data dissimilarity between megabiomes, a map-based statistic called ΔV (Sykes et al., 1999; Ni et al., 2000) was applied here (detailed information is in the methodology section).

Fig. S8 shows the dissimilarity between simulations and observations for megabiomes during MH, with the overall values for ΔV ranging from 0.43 (HadGEM2-ES) to 0.55 (IPSL-CM5A-LR). According to the classification of ΔV (see in the methodology section) for the 13 models, 12 (all except HadGEM2-ES) showed poor agreement with the observed vegetation distribution. Most models poorly simulate the desert, grassland and tropical forest areas for both periods, but perform better for warm mixed forest, tundra and temperate forest. However, this statistic is based on a point-to-point comparison and so the ΔV calculated here cannot represent an estimation of full vegetation simulation due to the uneven distribution of pollen data and the potentially huge difference in area of each megabiome. For instance, tundra in our data for PI is represented by only 4 points, which counts for a small contribution to the

ΔV since we averaged it over a total of 159 points, but this calculation could induce a significant bias if these 4 points cover a large area of China.

So, we used the biome scores based on the artificial neural network technique as described by Guiot et al. (1996) for interpolation (the plots in red rectangle in Fig. 5), and compared the simulated vegetation distribution from BIOME4 for each model with the interpolated pattern. During MH, most models are able to capture the tundra on the Tibetan Plateau as well as the combination of warm mixed forest and temperate forest in the southeast. However, all models fail to simulate or underestimate the desert area in the northwest compared to reconstructed data. The main model-data inconsistency in MH vegetation distribution occurs in the northeast, where data show a mix of grassland and temperate forest, and the models show a mix of grassland and boreal forest.

The area statistic carried out for simulated vegetation changes (Fig. 6) reveals that the main difference during MH, compared with PI, is that grassland replaced boreal forest in large tracts of the northeast (Fig. 5, Fig. S7). No other significant difference in vegetation distribution between the two periods was derived from models. Unlike in models, three main changes in megabiomes during MH are depicted by the data. Firstly, the megabiomes converted from grassland to temperate forest in the northeast. Secondly, a large area of temperate forest was replaced in the southeast by a northward expansion of warm mixed forest. Thirdly, in the northwest and at the northern margin of the Tibetan Plateau, part of the desert area changed into grassland. However, none of the models succeed in capturing these features, especially the enhanced vegetation conditions in the northeast during MH. Therefore, this failure to capture vegetation changes between the two periods will lead to a cumulating inconsistency in the model-data comparison for climate anomalies because of the vegetation-climate feedbacks.

Clim. Past Discuss., https://doi.org/10.5194/cp-2018-145
Manuscript under review for journal Clim. Past
Discussion started: 13 November 2018

4. Conclusion and Discussion

In response to the seasonal insolation change prescribed in PMIP3 for MH, all models produce similar large-scale patterns for seasonal temperature and precipitation (wetter and warmer in MTWA, colder in MTCO), with either an over- or underestimate of the climate changes when compared to the data. The main discrepancy emerging from the model-data comparison occurs in the annual and MTCO temperature, where data show an increased trend and most models (except CNRM-CM5 and HadGEM2-ES) simulate the opposite. Besides the qualitative consistency among models, triggered by the protocol of PIMIP3 experiments (Table 2), a variability in the magnitude of anomalies between models is clearly illustrated by the column bars (Fig.3 and Fig.4). These disparities in value or even pattern between models reflect the obvious differences in the response by the climate models to the MH forcing which shed light on the question of the magnitude of feedbacks among models.

As positive feedbacks between climate and vegetation are important to explain regional climate changes, the failure to capture or the underestimation of the amplitude of the observed vegetation differences among models (see Section 3.2) could amplify and partly account for the model-data disparities in climate change, mainly due to variations in the albedo. Because the HadGEM2-ES and HadGEM2-CC are the only two models in PMIP3 with dynamic vegetation simulation for MH, we thus focused on them to examine the variations in vegetation fraction in the simulations. The main vegetation changes during MH demonstrated by HadGEM2-ES are increased tree coverage (~15%) and a decreased bare soil fraction (~6%), while HadGEM2-CC depicts a ~3% decrease in tree fraction and a ~1% increase in bare soil (Fig. S9). We made a rough calculation of albedo variance caused solely by vegetation change for both two models and for our reconstruction, based on the area fraction and albedo value of each vegetation type (Betts, 2000; Bonfils et al., 2001; Oguntunde et al., 2006; Bonan, 2008).

Reconstruction showed vegetation changes during MH leading to a ~1.8% decrease in albedo when snow-free, with a much larger impact (~4.2% decrease) when snow-covered. The results from HadGEM2-ES are highly consistent with the albedo changes from the reconstruction, featuring a ~1.4% (~6.5%) decrease without (with) snow, while HadGEM2-CC produces an increased albedo value during MH (~0.22% for snow-free, ~1.9% with snow-cover), depending on its vegetation simulation. Two ideas could be inferred from this calculation, 1) HadGEM2-ES is much better in simulating the MH vegetation changes than HadGEM2-CC. 2) the failure by models to capture these vegetation changes will result in a much larger impact on winter albedo (with snow) than summer albedo (without snow).

These surface albedo changes due to vegetation changes could have a cumulative effect on the regional climate by modifying the radiative fluxes. For instance, the spread of trees into the grassland biome in the northeast during MH, revealed by the reconstruction in our study, will act as a positive feedback to climate warming by increasing the surface net shortwave radiation associated with reductions in albedo due to taller and darker canopies (Chapin et al., 2005). Previous studies show that cloud and surface albedo feedbacks on radiation are major drivers of differences between model outputs for past climates. Moreover, the land surface feedback shows large disparities among models (Braconnot and Kageyama, 2015).

We used a simplified approach (Tyler et al., 2007) to quantify the feedbacks and to compare model behavior for MH, thus justifying the focus on surface albedo and atmospheric scattering (mainly accounting for cloud change). Surface albedo and cloud change are calculated using the simulated incoming and outgoing radiative fluxes at the Earth's surface and at the top of atmosphere (TOA), based on data for the last 30 years averaged from all models. Using this framework, we quantified the effect of changes in albedo on the net shortwave flux at TOA (Braconnot and Kageyama, 2015), and further investigated the relationship between these changes and temperature change. Fig.7 shows that most models produced a negative cloud cover and surface albedo feedback on the annual mean shortwave radiative forcing. Concerning seasonal change, the shortwave cloud and surface feedback in most models tend to counteract the insolation forcing during the boreal summer, while they enhance the solar forcing during winter. A strong positive correlation between albedo feedback and temperature change is depicted, with a large spread in the models owing to the difference in albedo in the 13 models. In particular, CNRM-CM5 and HadGEM2-ES capture higher values of cloud and surface albedo feedback, which could be the reason for the reversal of the annual cooling trend seen in other models (Fig. 3d).

Although the MH remains an ideal target for model-data comparison, the PMIP exercise only allows the atmosphere and ocean response to be computed for seasonal forcing. In this study, we show that the model-data inconsistency for temperature is mainly because we are not able to simulate the MH vegetation and its interaction with climate through radiative and hydrological forcing with albedo. These results pinpoint the value of building a new generation of models able to capture not only the atmosphere and ocean response, but also the non-linear responses of vegetation and hydrology.

Besides the uncertainties in the models, IVM, from the data perspective, relies heavily on BIOME4, and since BIOME4 is a global vegetation model, it is possible that the spatial robustness of regional reconstruction could be less than that of global reconstruction due to the failure to simulate local features (Bartlein et al., 2011). China, located in the Asian monsoon area, has some specialized vegetation types which call for an improved ability to simulate regional vegetation in BIOME4. Of course, more reconstruction studies using multiple proxies and reliable methods are also required to narrow the discrepancies between data and model results.

Data availability

The PMIP3 output is publicly available at website (http://pmip3.lsce.ipsl.fr/) by the climate modelling groups, the 65 pollen biomization results are provided by Members of China Quaternary Pollen Data Base, Table 1 shows the information (including references) of the 91 collected pollen records and 3 original ones in our study. The full datasets of pollen are available upon the request to the corresponding author.

Author contribution

Yating Lin carried out the model-data analysis and prepared for the first manuscript, Gilles Ramstein contributed a lot to the paper's structure and content, Haibin Wu provided the reconstruction results from IVM and contributed the paper's structure and content. Raj Rani-Singh conducted the BIOME4 simulations. Pascale Braconnot, Masa Kegeyama and Zhengtang Guo contributed great ideas on model-data comparison work. Qin Li and Yunli Luo provided pollen data. All co-authors helped to improve the paper.

Competing interest

The authors declare no competing interests.

Acknowledgements

We acknowledge the World Climate Research Program's Working Group on Coupled Modelling, which is responsible for PMIP/CMIP, and we thank the climate modelling groups for producing and making available their model output. This research was funded by the Sino-French Caiyuanpei Program, the National Basic Research Program of China (Grant no. 2016YFA0600504), the National Natural Science Foundation of China (Grant nos. 41572165, 41690114, and 41125011), and the Bairen Programs of the Chinese Academy of Sciences.

References

An, C., Zhao, J., Tao, S., Lv, Y., Dong, W., Li, H., Jin, M., and Wang, Z.: Dust variation recorded by lacustrine sediments from arid Central Asia since ~ 15 cal ka BP and its implication for atmospheric circulation, Quaternary Research, 75, 566-573, 2011

Bartlein, P. J., Harrison, S. P., Brewer, S., Connor, S., Davis, B. A. S., Gajewski, K., Guiot, J., Harrison-Prentice, T. I., Henderson, A., Peyron, O., Prentice, I. C., Scholze, M., Seppä, H., Shuman, B., Sugita, S., Thompson, R. S., Viau, A. E., Williams, J., and Wu, H.B.: Pollen-based continental climate reconstructions at 6 and 21ka: a global synthesis, Climate Dynamics, 37, 775-802, 2011.

Berger, A.: Long-Term Variations of Daily Insolation and Quaternary Climatic Changes, Journal of the Atmospheric Sciences, 35, 2362-2367, 1978.

Betts, R. A.: Offset of the potential carbon sink from boreal forestation by decreases in surface albedo, Nature, 408, doi: 10.1038/nature. 35041545, 2000.

Bonan, G. B.: Forests and Climate Change: Forcings, Feedbacks, and the Climate Benefits of Forests, Science, 320, 1444-1449, 2008.

Bonfils, C., de Noblet-Ducoudré, N, Braconnot, P., and Joussaume, S.: Hot Desert Albedo and Climate Change: Mid-Holocene Monsoon in North Africa, Journal of Climate, 14, 3724–3737, 2001.

Braconnot, P., and Kageyama, M.: Shortwave forcing and feedbacks in Last Glacial Maximum and Mid-Holocene PMIP3 simulations, Philosophical Transactions of the Royal Society A: Mathematical, Physical and Engineering Sciences, 373, 2054-2060, 2015.

Braconnot, P., Harrison, S. P., Kageyama, M., Bartlein, P. J., Masson-Delmotte, V., Abe-Ouchi, A., Otto-Bliesner, B., and Zhao, Y.: Evaluation of climate models using palaeoclimatic data: Nature Climate Change, 2, 417-421, 2012.

Braconnot, P., Otto-Bliesner, B., Harrison, S., Joussaume, S., Peterchmitt, J. Y., Abe-Ouchi, A., Crucifix, M., Driesschaert, E., Fichefet, T., Hewitt, C. D., Kageyama, M., Kitoh, A., Laine, A., Loutre, M. F., Marti, O., Merkel, U., Ramstein, G., Valdes, P., Weber, S. L., Yu, Y., and Zhao, Y.: Results of PMIP2 coupled simulations of the Mid-Holocene and Last Glacial Maximum-Part 1: experiments and large-scale features, Clim. Past, 3, 261-277, 2007a.

Braconnot, P., Otto-Bliesner, B., Harrison, S., Joussaume, S., Peterschmitt, J. Y., Abe-Ouchi, A., Crucifix, M., Driesschaert, E., Fichefet, T., Hewitt, C. D., Kageyama, M., Kitoh, A., Loutre, M. F., Marti, O., Merkel, U., Ramstein, G., Valdes, P., Weber, L., Yu, Y., and Zhao, Y.: Results of PMIP2 coupled simulations of the Mid-Holocene and Last Glacial Maximum-Part 2: feedbacks with emphasis on the location of the ITCZ and mid- and high latitudes heat budget, Clim. Past, 3, 279-296, 2007b.

Caudill, M., Bulter, C.: Understanding Neural Networks, Basic Networks, 1, 309, 1992.

Chapin, F. S., Sturm, M., Serreze, M. C., McFadden, J. P., Key, J. R., Lloyd, A. H., McGuire, A. D., Rupp, T. S., Lynch, A. H., Schimel, J. P., Beringer, J., Chapman, W. L., Epstein, H. E., Euskirchen, E. S., Hinzman, L. D., Jia, G., Ping, C.L., Tape, K. D., Thompson, C. D. C., Walker, D. A., and Welker, J. M.: Role of Land-Surface Changes in Arctic Summer Warming, Science, 310, 657-660, 2005.

Chen, F., Cheng, B., Zhao, Y., Zhu, Y., and Madsen, D. B.: Holocene environmental change inferred from a high-resolution pollen record, Lake Zhuyeze, arid China, The Holocene, 16, 675-684, 2006.

Chen, F., Xu, Q., Chen, J., Birks, H. J. B., Liu, J., Zhang, S., Jin, L., An, C., Telford, R. J., Cao, X., Wang, Z., Zhang, X., Selvaraj, K., Lu, H., Li, Y., Zheng, Z., Wang, H., Zhou, A., Dong, G., Zhang, J., Huang, X., Bloemendal, J., and Rao, Z.: East Asian summer monsoon precipitation variability since the last deglaciation, Scientific Reports, 5, 11186, 2015.

Cheng, H., Edwards, R. L., Sinha, A., Spötl, C., Yi, L., Chen, S., Kelly, M., Kathayat, G., Wang, X., Li, X., Kong, X., Wang, Y., Ning, Y., and Zhang, H.: The Asian monsoon over the past

640,000 years and ice age terminations, Nature, 534, 640, 2016.

Cui, M., Luo, Y., and Sun, X.: Paleovegetational and paleoclimatic changed in Ha'ni Lake, Jilin since 5ka BP, Marine Geology & Quaternary Geology, 26, 117-122, 2006 (in Chinese).

Davis, B. A. S., Brewer, S., Stevenson, A. C., and Guiot, J.: The temperature of Europe during the Holocene reconstructed from pollen data, Quaternary Science Reviews, 22, 1701-1716, 2003.

Farrera, I., Harrison, S. P., Prentice, I. C., Ramstein, G., Guiot, J., Bartlein, P. J., Bonnefille, R., Bush, M., Cramer, W., von Grafenstein, U., Holmgren, K., Hooghiemstra, H., Hope, G., Jolly, D., Lauritzen, S. E., Ono, Y., Pinot, S., Stute, M., and Yu, G.: Tropical climates at the Last Glacial Maximum: a new synthesis of terrestrial palaeoclimate data. I. Vegetation, lake-levels and geochemistry, Climate Dynamics, 15, 823-856, 1999.

Fischer, N., and Jungclaus, J. H.: Evolution of the seasonal temperature cycle in a transient Holocene simulation: orbital forcing and sea-ice, Clim. Past, 7, 1139-1148, 2011.

Ganopolski, A., Kubatzki, C., Claussen, M., Brovkin, V., and Petoukhov, V.: The Influence of Vegetation-Atmosphere-Ocean Interaction on Climate During the Mid-Holocene, Science, 280, 1916-1919, 1998.

Guiot, J., and C. Goeury.: PPPBASE, a software for statistical analysis of paleoecological and paleoclimatological data, Dendrochronologia, 14, 295-300, 1996.

Guiot, J., Torre, F., Jolly, D., Peyron, O., Boreux, J. J., and Cheddadi, R.: Inverse vegetation modeling by Monte Carlo sampling to reconstruct palaeoclimates under changed precipitation seasonality and CO2 conditions: application to glacial climate in Mediterranean region, Ecological Modelling, 127, 119-140, 2000.

Guo, L., Feng, Z., Lee, X., Liu, L., and Wang, L.: Holocene climatic and environmental changes recorded in Baahar Nuur Lake in the Ordos Plateau, Southern Mongolia of china, Chinese Science Bulletin, 52, 959-966, 2007.

H Bigelow, N., Brubaker, L., Edwards, M., Harrison, S., Prentice, I., Anderson, P., Andreev, A., Bartlein, P., Christensen, T. R., Cramer, W., Kaplan, J., Anatoly, L., V. Matveyeva, N., Murray, D., David McGuire, A., Razzhivin, V., Ritchie, J., Smith, B., A Walker, D., and S. Volkova, V.: Climate change and Arctic ecosystems. I. Vegetation changes north of 55°N between the Last Glacial Maximum, mid-Holocene and present, 2003.

Hargreaves, J. C., Annan, J. D., Ohgaito, R., Paul, A., and Abe-Ouchi, A.: Skill and reliability of climate model ensembles at the Last Glacial Maximum and mid-Holocene, Clim. Past, 9, 811-823, 2013.

Harrison, S. P., Bartlein, P. J., Brewer, S., Prentice, I. C., Boyd, M., Hessler, I., Holmgren, K., Izumi, K., and Willis, K.: Climate model benchmarking with glacial and mid-Holocene climates, Climate Dynamics, 43, 671-688, 2014.

Harrison, S. P., Bartlein, P. J., K., Izumi, Li, G., Annan, J., Hargreaves, J., Braconnot, P., and Kageyama, M.: Evaluation of CMIP5 paleo-simulations to improve climate projections, Nature Climate Change, 5, 735-743, 2015.

Harrison, S., P., Braconnot, P., Hewitt, C., and Stouffer, R., J.: Fourth International Workshop of the Palaeoclimate Modelling Intercomparison Project (PMIP): Lauching PMIP2 Phase II, EOS, 83, 447-457, 2002.

Herzschuh, U., Kramer, A., Mischke, S., and Zhang, C.: Quantitative climate and vegetation trends since the late glacial on the northeastern Tibetan Plateau deduced from Koucha Lake pollen spectra, Quaternary Research, 71, 162-171, 2009.

Herzschuh, U., Kürschner, H., and Mischke, S.: Temperature variability and vertical vegetation belt shifts during the last ~50,000 yr in the qilian mountains (ne margin of the tibetan plateau, china), Quaternary Research, 66, 133-146, 2006.

Jia, L., and Zhang, Y.: Studies on Palynological assemblages and paleoenvironment of late Quaternary on the east margin of the Chanjiang (Yangtze) river delta, Acta Micropalaeontologica Sinica, 23, 70-76, 2006 (in Chinese).

Jiang, D., Lang, X., Tian, Z., and Wang, T.: Considerable Model–Data Mismatch in Temperature over China during the Mid-Holocene: Results of PMIP Simulations, Journal of Climate, 25, 4135-4153, 2012.

Jiang, Q., and Piperno., R. D.: Environmental and archaeological implications of a late Quaternary palynological sequence, Poyang lake, Southern China, Quaternary Research, 52, 250-258, 1999.

Jiang, W., Guiot, J., Chu, G., Wu, H., Yuan, B., Hatté, C., and Guo, Z.: An improved methodology of the modern analogues technique for palaeoclimate reconstruction in arid and semi-arid regions, Boreas, 39, 145-153, 2010.

Jiang, W., Guo, Z., Sun, X., Wu, H., Chu, G., Yuan, B., Hatte, C., and Guiot, J.: Reconstruction of climate and vegetation changes of lake bayanchagan (inner mongolia): holocene variability of the east asian monsoon. Quaternary Research, 65, 411-420, 2006.

Jiang, W., Leroy, S. G., Ogle, N., Chu, G., Wang, L., and Liu, J.: Natural and authropogenic forest fires recorded in the Holocene pollen record from a Jinchuan peat bog, northeastern China, Palaeogeography, Palaeoclimatology, Palaeoecology, 261, 47-57, 2008.

Joussaume, S., and Taylor, K. E.: Status of the Paleoclimate Modeling Intercomparison Project, Proc. 1st Int. AMIP Scientific Conf, 425-430, 1995.

Joussaume, S., Taylor, K. E., Braconnot, P., Mitchell, J. F. B., Kutzbach, J. E., Harrison, S. P.,

Clim. Past Discuss., https://doi.org/10.5194/cp-2018-145
Manuscript under review for journal Clim. Past
Discussion started: 13 November 2018

Prentice, I. C., Broccoli, A. J., Abe-Ouchi, A., Bartlein, P. J., Bonfils, C., Dong, B., Guiot, J., Herterich, K., Hewitt, C. D., Jolly, D., Kim, J. W., Kislov, A., Kitoh, A., Loutre, M. F., Masson, V., McAvaney, B., McFarlane, N., de Noblet, N., Peltier, W. R., Peterschmitt, J. Y., Pollard, D., Rind, D., Royer, J. F., Schlesinger, M. E., Syktus, J., Thompson, S., Valdes, P., Vettoretti, G., Webb, R. S., Wyputta, U.: Monsoon changes for 6000 years ago: Results of 18 simulations from the Paleoclimate Modeling Intercomparison Project (PMIP), Geophysical Research Letters, 26, 856-862, 1999.

Kaplan, J. O., Bigelow, N. H., Bartlein, P. J., Christensen, T. R., Cramer, W., Harrison, S. P., Matveyeva, N. V., McGuire, A. D., Murray, D. F., Prentice, I. C., Razzhivin, V. Y., Smith, B., Anderson, P. M., Andreev, A. A., Brubaker, L. B., Edwards, M. E., and Lozhkin, A. V.: Climate change and Arctic ecosystems II: Modeling, palaeodata-model comparisons, and future projections, Journal of Geophysical Research: Atmospheres, 108, 2003.

Kohfeld, K. E. and Harrison, S.: How well we can simulate past climates? Evaluating the models using global palaeoenvironmental datasets, Quaternary Science Reviews, 19, 321-346, 2000.

Lee, Y., and Liew, M.: Pollen stratigraphy, vegetation and environment of the last glacial and Holocene-A record from Toushe Basin, central Taiwan, Palaeogeography, Palaeoclimatology, Palaeoecology, 287, 58-66, 2010.

Li, C., Wu, Y., and Hou, X.: Holocene vegetation and climate in Northeast China revealed from Jingbo Lake sediment, Quaternary International, 229, 67-73, 2011.

Li, Q., Wu, H., Guo, Z., Yu, Y., Ge, J., Wu, J., Zhao, D., and Sun, A.: Distribution and vegetation reconstruction of the deserts of northern China during the mid-Holocene, Geophysical Reserch Letter, 41, 2184-5191, 2014.

Clim. Past Discuss., https://doi.org/10.5194/cp-2018-145
Manuscript under review for journal Clim. Past
Discussion started: 13 November 2018

Li, X., Zhao, K., Dodson, J., and Zhou, X.: Moisture dynamics in central Asia for the last 15 kyr: new evidence from Yili Valley, Xinjiang, NW China, Quaternary Science Reviews, 30, 23-34, 2011.

Li, X., Zhou, J., and Dodson, J,: The vegetation characteristics of the ‘ yuan ’ area at yaoxian on the loess plateau in china over the last 12 000 years. Review of Palaeobotany & Palynology, 124, 1-7, 2003.

Liew, M., Huang, Y., and Kuo, M.: Pollen stratigraphy, vegetation and environment of the last glacial and Holocene-A record from Toushe Basin, central Taiwan, Quaternary International, 14, 16-33, 2006.

Liu, J., Zhao, S., Cheng, J., Bao, J., and Yin, G.: A study of vegetation and climate evolution since the Holocene near the banks of the Qiangtang River in Hangzhou Bay, Earth Science Frontiers, 5, 235-245, 2007 (in Chinese).

Liu, Y., Liu, J., and Han, J.: Pollen record and climate changing since 12.0ka B. P. in Erlongwan Maar Lake, Jilin province, Journal of Jilin University (Earth Science Edition), 39, 93-98, 2009 (in Chinese).

Liu, Y., Zhang, S., Liu, J., You, H., and Han, J.: Vegetation and environment history of erlongwan Maar lake during the late Pleistocene on pollen record, Acta Micropalaeontologica Sinica, 25, 274-280, 2008 (in Chinese).

Liu, Z., Harrison, S. P., Kutzbach, J. E., and Otto-Bliesner, B.: Global monsoons in the mid-Holocene and oceanic feedback, Climate Dynamics, 22, 157-182, 2004.

Liu, Z., Wang, Y., Gallimore, R., Gasse, F., Johnson, T., deMenocal, P., Adkins, J., Notaro, M., Prentice, I.C., Kutzbach, J., Jacob, R., Behling, P., Wang, L., and Ong, E.: Simulating the transient evolution and abrupt change of Northern Africa atmosphere–ocean–terrestrial ecosystem in the Holocene, Quaternary Science Reviews, 26, 1818-1837, 2007.

Liu, Z., Zhu, J., Rosenthal, Y., Zhang, X., Otto-Bliesner, B. L., Timmermann, A., Smith, R. S., Lohmann, G., Zheng, W., and Elison Timm, O.: The Holocene temperature conundrum, Proceedings of the National Academy of Sciences, 111, E3501-E3505, 2014.

Lu, H., Wu, N., Liu, K.-b., Zhu, L., Yang, X., Yao, T., Wang, L., Li, Q., Liu, X., Shen, C., Li, X., Tong, G., and Jiang, H.: Modern pollen distributions in Qinghai-Tibetan Plateau and the development of transfer functions for reconstructing Holocene environmental changes, Quaternary Science Reviews, 30, 947-966, 2011.

Mann, M. E., Zhang, Z., Hughes, M. K., Bradley, R. S., Miller, S. K., Rutherford, S., and Ni, F.: Proxy-based reconstructions of hemispheric and global surface temperature variations over the past two millennia, Proceedings of the National Academy of Sciences, 105, 13252-13256, 2008.

Marchant, R., Cleef, A., Harrison, S. P., Hooghiemstra, H., Markgraf, V., Van Boxel, J., Ager, T., Almeida, L., Anderson, R., Baied, C., Behling, H., Berrio, J. C., Burbridge, R., Bjorck, S., Byrne, R., Bush, M., Duivenvoorden, J., Flenley, J., De Oliveira, P., Van Gee, B., Graf, K., Gosling, W. D., Harbele, S., Van Der Hammen, T., Hansen, B., Horn, S., Kuhry, P., Ledru, M. P., Mayle, F., Leyden, B., Lozano-Garcia, S., Melief, A. M., Moreno, P., Moar, N. T., Prieto, A., Van Reenen, G., Salgado-Labouriau, M., Schabitz, F., Schreve-Brinkman, E. J., and Wille, M.: Pollen-based biome reconstructions for Latin America at 0, 6000 and 18 000 radiocarbon years ago, Climate of the Past, 5, 725-767, 2009.

Marcott, S., Shakun, J., U Clark, P., and Mix, A.: A Reconstruction of Regional and Global Temperature for the Past 11,300 Years, Sciecnce, 1198-1201, 2013.

Mauri, A., Davis, B. A. S., Collins, P. M., and Kaplan, J. O.: The climate of Europe during the Holocene: a gridded pollen-based reconstruction and its multi-proxy evaluation, Quaternary Science Reviews, 112, 109-127, 2015.

Members of the China Quaternary Pollen Data base.: Pollen-based Biome reconstruction at

Clim. Past Discuss., https://doi.org/10.5194/cp-2018-145
Manuscript under review for journal Clim. Past
Discussion started: 13 November 2018

Middle Holocene (6ka BP) and Last Glacial Maximum (18ka BP) in China, Acta Botanica Sinica, 42, 1201-1209, 2000.

Members, M. P.: Constraints on the magnitude and patterns of ocean cooling at the Last Glacial Maximum, Nature Geoscience, 2, 127-130, 2009.

Ni, J., Sykes, M. T., Prentice, I. C., and Cramer, W.: Modelling the vegetation of China using the process-based equilibrium terrestrial biosphere model BIOME3, Global Ecology and Biogeography, 9, 463-479, 2000.

Oguntunde, P. G., Ajayi, A. E., and Giesen, N.: Tillage and surface moisture effects on bare-soil albedo of a tropical loamy sand, Soil and Tillage Research, 85, 107-114, 2006.

O'ishi, R., A. Abe - Ouchi, I. C. Prentice, and S. Sitch.: Vegetation dynamics and plant CO2 responses as positive feedbacks in a greenhouse world, Geophysical Research Lettters, v. 36, L11706, doi: 10.1029/2009GL038217, 2009.

Otto, J., T. Raddatz, M. Claussen, V. Brovkin, and V. Gayler.: Separation of atmosphere-ocean-vegetation feedbacks and synergies for mid-Holocene climate, Geophysical Research Lettters, 36, L09701, doi: 10.1029/2009GL037482, 2009.

Peyron, O., Guiot, J., Cheddadi, R., Tarasov, P., Reille, M., De Beaulieu, J.L., Bottema,

Peyron, O., Jolly, D., Bonnefille, R., Vincens, A., and Guiot, J.: Climate of East Africa 6000 ^{14}C Yr B.P. as Inferred from Pollen Data, Quaternary Research, 54, 90-101, 2000.

Pickett Elizabeth, J., Harrison Sandy, P., Hope, G., Harle, K., Dodson John, R., Peter Kershaw, A., Colin Prentice, I., Backhouse, J., Colhoun Eric, A., D'Costa, D., Flenley, J., Grindrod, J., Haberle, S., Hassell, C., Kenyon, C., Macphail, M., Martin, H., Martin Anthony, H., McKenzie, M., Newsome Jane, C., Penny, D., Powell, J., Ian Raine, J., Southern, W., Stevenson, J., Sutra, J. P., Thomas, I., Kaars, S., and Ward, J.: Pollen-based reconstructions of biome distributions for Australia, Southeast Asia and the Pacific (SEAPAC region) at 0, 6000 and 18,000 ^{14}C yr BP, Journal of Biogeography, 31, 1381-1444, 2004.

pollen data, Quaternary Research. 49, 183–196, 1998.

Prentice, I. C., and Jolly, D.: Mid-Holocene and glacial-maximum vegetation geography of the northern continents and Africa, Journal of Biogeography, 27, 507-519, 2001.

S., Andrieu, V.: Climatic reconstruction in Europe for 18 000 year B.P. from

Shakun, J. D., Clark, P. U., He, F., Marcott, S. A., Mix, A. C., Liu, Z., Otto-Bliesner, B., Schmittner, A., and Bard, E.: Global warming preceded by increasing carbon dioxide concentrations during the last deglaciation, Nature, 484, 49, 2012.

Shen, C., Liu, K., Tang, L., Overpeck, J. T.: Quantitative relationships between modern pollen rain and climate in the Tibetan Plateau, Review of Palaeobotany and Palynology, 140, 61-77, 2006.

Shen, J., Jones, R. T., Yang, X., Dearing, J. A., and Wang, S.: The holocene vegetation history of lake erhai, yunnan province southwestern china: the role of climate and human forcings, Holocene, 16, 265-276, 2006.

Shu, Q., Xiao, J., Zhang, M., Zhao, Z., Chen, Y., and Li, J.:

Sun. X., Wang. F., and Sun. C.: Pollen-climate response surfaces of selected taxa from Northern China, Science in China Series D-Earth Sciences, 39, 486, 1996.

Swann, A. L., Fung, I. Y., Levis, S., Bonan, G. B., and Doney, S. C.: Changes in Arctic vegetation amplify high-latitude warming through the greenhouse effect, Proceedings of the National Academy of Sciences, 107, 1295-1300, 2010.

Sykes, M.T., Prentice, I.C., and Laarif, F.: Quantifying the impact of global climate change on potential natural vegetation, Climatic Change, 41, 37–52, 1999.

Tropical Pacific Ocean, Science, 344, 84, 2014.

Tylor, K.E., Crucifix, M., Braconnot, P., Hewitt, C. D., Doutriaux. C., Broccoli, A. J., Mitchell, J. F. B., Webb, M. J.: Estimating shortwave radiative forcing and response in climate models, J. Clim, 20, 2530-2543, 2007.

Wang, H., Liu, H., Zhu, J., and Yin, Y.: Holocene environmental changes as recorded by mineral magnetism of sediments from Anguli-nuur Lake, southeastern Inner Mongolia Plateau, China, Palaeogeography, Palaeoclimatology, Palaeoecology, 285, 30-49, 2010.

Wang, X., Zhang, G., Li, W., Zhang, X., Zhang, E., and Xiao, X.: Environmental changes during early-middle holocene from the sediment record of the chaohu lake, anhui province, Chinese Science Bulletin, 53, 153-160, 2008.

Webb, T. I.: Global paleoclimatic data base for 6000 yr BP, Brown Univ., Providence, RI (USA). Dept. of Geological Sciences, DOE/EV/10097-6; Other: ON: DE85006628 United States Other: ON: DE85006628 NTIS, PC A08/MF A01. HEDB English, 1985.

Wen, R., Xiao, J., Chang, Z., Zhai, D., Xu, Q., Li, Y. and Itoh, S.: Holocene precipitation and temperature variations in the East Asian monsoonal margin from pollen data from Hulun Lake in northeastern Inner Mongolia, China, Boreas, 39, 262-272, 2010.

Wischnewski, J., Mischke, S., Wang, Y., and Herzschuh, U.: Reconstructing climate variability on the northeastern Tibetan Plateau since the last Lateglacial – a multi-proxy, dual-site approach comparing terrestrial and aquatic signals, Quaternary Science Reviews, 30, 82-97, 2011.

Wohlfahrt, J., Harrison, S. P., and Braconnot, P.: Synergistic feedbacks between ocean and vegetation on mid- and high-latitude climates during the mid-Holocene, Climate Dynamics, 22, 223-238, 2004.

Wu, H., Guiot, J., Brewer, S., and Guo, Z.: Climatic changes in Eurasia and Africa at the last glacial maximum and mid-Holocene: reconstruction from pollen data using inverse vegetation modeling, Climate Dynamics, 29, 211-229, 2007.

Wu, H., Luo, Y., Jiang, W., Li, Q., Sun, Ai., and Guo, Z.: Paleoclimate reconstruction from pollen data using inverse vegetation approach: Validation of model using modern data, 36, 520-529 (in Chinese), 2016.

Xia, Y.: Preliminary study on vegetational development and climatic changes in the Sanjiang Plain in the last 12000 years, Scientia Geographica Sinica, 8, 241-249, 1988 (in Chinese).

Xia, Z., Chen, G., Zheng, G., Chen, F., and Han, J.: Climate background of the evolution from Paleolithic to Neolithic cultural transition during the last deglaciation in the middle reaches of the Yellow River, Chinese Science Bulletin, 47, 71-75, 2002.

Xiao, J., Xu, Q., Nakamura, T., Yang, X., Liang, W., and Inouchi, Y.: Holocene vegetation variation in the Daihai Lake region of north-central China: a direct indication of the Asian monsoon climatic history, Quaternary Science Reviews, 23, 1669-1679, 2004.

Xiao, X., Haberle, S. G., Shen, J., Yang, X., Han, Y., Zhang, E., and Wang, S.: Latest Pleistocene and Holocene vegetation and climate history inferred from an alpine lacustrine record, northwestern Yunnan Province, southwestern China, Quaternary Science reviews, 86, 35-48, 2014.

Xue, S., and Li, X.: Holocene vegetation characteristics of the southern loess plateau in the weihe river valley in china, Review of Palaeobotany & Palynology, 160 46-52, 2010.

Yang, Y., and Wang, S.: Study on mire development and paleoenvironment change since 8.0ka B.P. in the northern part of the Sangjiang Plain, Scientia Geographica Sinica, 23, 32-38, 2003 (in Chinese).

Yu, L., Wang, N., Cheng, H., Long, H., and Zhao, Q.: Holocene environmental change in the marginal area of the asian monsoon: a record from zhuye lake, nw china, Boreas, 38, 349-361, 2010.

Zhang, Y. G., Pagani, M., and Liu, Z.: A 12-Million-Year Temperature History of the

Zhang, Y., Jia, L., and Lyu, B.: Studies on Evolution of Vegetation and Climate since 7000 Years ago in Estuary of Changjiang River Region, Marine Science Bulletin, 3, 27-34, 2004 (in Chinese).

Zhang, Z., Xu, Q., Li, Y., Yang, X., Jin, Z., and Tang, J.: Environmental changes of the Yin ruins area based on pollen analysis, Quaternary Science, 27, 461-468, 2007 (in Chinese).

Zhao, Y., Yu, Z., Chen, F., Ito, E., and Zhao, C.: Holocene vegetation and climate history at Hurleg Lake in the Qaidam Basin, northwest China, Review of Palaeobotany and palynology, 145, 275-288, 2007.

Zhou, J., Liu, D., Zhuang, Z., Wang, Z., and Liu, L.: The sediment layers and the records of the Paleoenvironment in the Chaoyanggang Lagoon,Rongcheng City of Shandong Province Since Holocene Transgression, Periodical of Ocean University of China, 38, 803-808, 2008 (in Chinese).

Zou, S., Cheng, G., Xiao, H., Xu, B., and Feng, Z.: Holocene natural rhythms of vegetation and present potential ecology in the western chinese loess plateau, Quaternary International, 194, 55-67, 2009.

717 **Table 1. Basic information of the pollen dataset used in this study**

Site	Lat	Lon	Alt	Webb 1-7	Source
Sujiawan	35.54	104.52	1700	2	original data
Xiaogou	36.10	104.90	1750	2	original data
Dadiwan	35.01	105.91	1400	1	original data
Sanjiaocheng	39.01	103.34	1320	1	Chen et al., 2006
Chadianpo	36.10	114.40	65	2	Zhang et al., 2007
Qindeli	48.08	133.25	60	2	Yang and Wang, 2003
Fuyuanchuangye	47.35	133.03	56	3	Xia, 1988
Jingbo Lake	43.83	128.50	350	2	Li et al., 2011
Hani Lake	42.22	126.52	900	1	Cui et al., 2006
Jinchuan	42.37	126.43	662	5	Jiang et al., 2008
Maar Lake	42.30	126.37	724	1	Liu et al., 2009
Maar Lake	42.30	126.37	724	1	Liu et al., 2008
Xie Lake SO4	37.38	122.52	0	1	Zhou et al., 2008
Nanhuiheming Core	31.05	121.58	7	2	Jia and Zhang, 2006
Toushe	23.82	120.88	650	1	Liu et al., 2006
Dongyuan Lake	22.17	120.83	415	2	Lee et al., 2010
Yonglong CY	31.78	120.44	5	3	Zhang et al., 2004
Hangzhou HZ3	30.30	120.33	6	4	Liu et al., 2007
Xinhua XH1	32.93	119.83	2	3	Shu et al., 2008
ZK01	31.77	119.80	6	2	Shu et al., 2007
Chifeng	43.97	119.37	503	2	Xu et al., 2002
SZK1	26.08	119.31	9	1	Zheng et al., 2002
Gucheng	31.28	118.90	6	4	Yang et al., 1996
Lulong	39.87	118.87	23	2	Kong et al., 2000
Hulun Lake	48.92	117.42	545	1	Wen et al., 2010
CH-1	31.56	117.39	5	2	Wang et al., 2008
Sanyi profile	43.62	117.38	1598	4	Wang et al., 2005
Xiaoniuchang	42.62	116.82	1411	1	Liu et al., 2002
Haoluku	42.87	116.76	1333	2	Liu et al., 2002
Liuzhouwan	42.71	116.68	1410	7	Liu et al., 2002
Poyang Lake 103B	28.87	116.25	16	4	Jiang and Piperno, 1999
Baiyangdian	38.92	115.84	8	2	Xu et al., 1988
Bayanchagan	42.08	115.35	1355	1	Jiang et al., 2006
Huangjiapu	40.57	115.15	614	7	Sun et al., 2001
Dingnan	24.68	115.00	250	2	Xiao et al., 2007
Guang1	36.02	114.53	56	1	Zhang et al., 2007
Angulinao	41.33	114.35	1315	1	Liu et al., 2010
Yangyuanxipu	40.12	114.22	921	6	Wang et al., 2003
Shenzhen Sx07	22.75	113.78	2	2	Zhang and Yu, 1999
GZ-2	22.71	113.51	1	7	Wang et al., 2010

Daihai99a	40.55	112.66	1221	2	Xiao et al., 2004
Daihai	40.55	112.66	1221	2	Sun et al., 2006
Sihenan profile	34.80	112.40	251	1	Sun and Xia, 2005
Diaojiaohaizi	41.30	112.35	2015	1	Yang et al., 2001
Ganhaizi	39.00	112.30	1854	3	Meng et al., 2007
Jiangling profile	30.35	112.18	37	1	Xie et al., 2006
Helingeer	40.38	111.82	1162	3	Li et al., 2011
Shennongjia2	31.75	110.67	1700	1	Liu et al., 2001
Huguangyan Maar Lake B	21.15	110.28	59	2	Wang et al., 2007
Yaoxian	35.93	110.17	1556	2	Li et al., 2003
Jixian	36.00	110.06	1005	6	Xia et al., 2002
Shennongjia Dajiu Lake	31.49	110.00	1760	2	Zhu et al., 2006
Qigainur	39.50	109.85	1300	1	Sun and Feng, 2013
Beizhuangcun	34.35	109.53	519	1	Xue et al., 2010
Lantian	34.15	109.33	523	1	Li and Sun, 2005
Bahanniao	39.32	109.27	1278	1	Guo et al., 2007
Midiwan	37.65	108.62	1400	1	Li et al., 2003
Jinbian	37.50	108.33	1688	2	Cheng, 2011
Xindian	34.38	107.80	608	1	Xue et al., 2010
Nanguanzhuang	34.43	107.75	702	1	Zhao et al., 2003
Xifeng	35.65	107.68	1400	3	Xu, 2006
Jiyuan	37.13	107.40	1765	3	Li et al., 2011
Jiacunyuan	34.27	106.97	1497	2	Gong, 2006
Dadiwan	35.01	105.91	1400	1	Zou et al., 2009
Maying	35.34	104.99	1800	1	Tang and An, 2007
Huiningxiaogou	36.10	104.90	1750	2	Wu et al., 2009
Sujiawan	35.54	104.52	1700	2	Zou et al., 2009
QTH02	39.07	103.61	1302	1	Yu et al., 2009
Laotanfang	26.10	103.20	3579	2	Zhang et al., 2007
Hongshui River2	38.17	102.76	1511	1	Ma, 2003,
Ruoergai	33.77	102.55	3480	1	Cai, 2006
Hongyuan	32.78	102.52	3500	2	Wang et al., 2006
Dahaizi	27.50	102.33	3660	1	Li et al., 1988
Shayema Lake	28.58	102.22	2453	1	Tang and Shen, 1996
Luanhaizi	37.59	101.35	3200	5	Herzschuh et al., 2006
Lugu Lake	27.68	100.80	2692	1	Zheng et al., 2014
Qinghai Lake	36.93	100.73	3200	2	Shen et al., 2004
Dalianhai	36.25	100.41	2850	3	Cheng et al., 2010
Erhai ES Core	25.78	100.19	1974	1	Shen et al., 2006
Xianmachi profile	25.97	99.87	3820	7	Yang et al., 2004
TCK1	26.63	99.72	3898	1	Xiao et al., 2014
Yidun Lake	30.30	99.55	4470	4	Shen et al., 2006

Kuhai lake	35.30	99.20	4150	1	Wischnewski et al., 2011
Koucha lake	34.00	97.20	4540	2	Herzschuh et al., 2009
Hurleg	37.28	96.90	2817	2	Zhao et al., 2007
Basu	30.72	96.67	4450	3	Tang et al., 1998
Tuolekule	43.34	94.21	1890	1	An et al., 2011
Balikun	43.62	92.77	1575	1	Tao et al., 2010
Cuona	31.47	91.51	4515	3	Tang et al., 2009
Dongdaohaizi2	44.64	87.58	402	1	Li et al., 2001
Bositeng Lake	41.96	87.21	1050	1	Xu, 1998
Cuoqin	31.00	85.00	4648	4	Luo, 2008
Yili	43.86	81.97	928	2	Li et al., 2011
Bangong Lake	33.75	78.67	4241	1	Huang et al., 1996
Shengli	47.53	133.87	52	2	CQPD, 2000
Qingdeli	48.05	133.17	52	1	CQPD, 2000
Changbaishan	42.22	126.00	500	2	CQPD, 2000
Liuhe	42.90	125.75	910	7	CQPD, 2000
Shuangyang	43.27	125.75	215	1	CQPD, 2000
Xiaonan	43.33	125.33	209	1	CQPD, 2000
Tailai	46.40	123.43	146	5	CQPD, 2000
Sheli	45.23	123.31	150	4	CQPD, 2000
Tongtu	45.23	123.30	150	7	CQPD, 2000
Yueyawan	37.98	120.71	5	1	CQPD, 2000
Beiwangxu	37.75	120.61	6	1	CQPD, 2000
East Tai Lake1	31.30	120.60	3	1	CQPD, 2000
Suzhou	31.30	120.60	2	7	CQPD, 2000
Sun-Moon Lake	23.51	120.54	726	2	CQPD, 2000
West Tai Lake	31.30	119.80	1	1	CQPD, 2000
Changzhou	31.43	119.41	5	1	CQPD, 2000
Dazeyin	39.50	119.17	50	7	CQPD, 2000
Hailaer	49.17	119.00	760	2	CQPD, 2000
Cangumiao	39.97	118.60	70	1	CQPD, 2000
Qianhuzhuang	40.00	118.58	80	6	CQPD, 2000
Reshuitang	43.75	117.65	1200	1	CQPD, 2000
Yangerzhuang	38.20	117.30	5	7	CQPD, 2000
Mengcun	38.00	117.06	7	5	CQPD, 2000
Hanjiang-CH2	23.48	116.80	5	2	CQPD, 2000
Hanjiang-SH6	23.42	116.68	3	7	CQPD, 2000
Hanjiang-SH5	23.45	116.67	8	2	CQPD, 2000
Hulun Lake	48.90	116.50	650	1	CQPD, 2000
Heitutang	40.38	113.74	1060	1	CQPD, 2000
Zhujiang delta PK16	22.73	113.72	15	7	CQPD, 2000
Angulitun	41.30	113.70	1400	7	CQPD, 2000
Bataigou	40.92	113.63	1357	1	CQPD, 2000

Dahewan	40.87	113.57	1298	2	CQPD, 2000
Yutubao	40.75	112.67	1254	7	CQPD, 2000
Zhujiang delta K5	22.78	112.63	12	1	CQPD, 2000
Da-7	40.52	112.62	1200	3	CQPD, 2000
Hahai-1	40.17	112.50	1200	5	CQPD, 2000
Wajianggou	40.50	112.50	1476	4	CQPD, 2000
Shuidong Core A1	21.75	111.07	-8	2	CQPD, 2000
Dajahu	31.50	110.33	1700	2	CQPD, 2000
Tianshuigou	34.87	109.73	360	7	CQPD, 2000
Mengjiawan	38.60	109.67	1190	7	CQPD, 2000
Fuping BK13	34.70	109.25	422	7	CQPD, 2000
Yaocun	34.70	109.22	405	2	CQPD, 2000
Jinbian	37.80	108.60	1400	4	CQPD, 2000
Dishaogou	37.83	108.45	1200	2	CQPD, 2000
Shuidonggou	38.20	106.57	1200	5	CQPD, 2000
Jiuzhoutai	35.90	104.80	2136	7	CQPD, 2000
Luojishan	27.50	102.40	3800	1	CQPD, 2000
RM-F	33.08	102.35	3400	2	CQPD, 2000
Hongyuan	33.25	101.57	3492	1	CQPD, 2000
Wasong	33.20	101.52	3490	1	CQPD, 2000
Guhu Core 28	27.67	100.83	2780	7	CQPD, 2000
Napahai Core 34	27.80	99.60	3260	2	CQPD, 2000
Lop Nur	40.50	90.25	780	7	CQPD, 2000
Chaiwobao1	43.55	87.78	1100	2	CQPD, 2000
Chaiwobao2	43.33	87.47	1114	1	CQPD, 2000
Manasi	45.97	84.83	257	2	CQPD, 2000
Wuqia	43.20	83.50	1000	7	CQPD, 2000
Madagou	37.00	80.70	1370	2	CQPD, 2000
Tongyu	44.83	123.10	148	5	CQPD, 2000
Nanjing	32.15	119.05	10	2	CQPD, 2000
Banpo	34.27	109.03	395	1	CQPD, 2000
QL-1	34.00	107.58	2200	7	CQPD, 2000
Dalainu	43.20	116.60	1290	7	CQPD, 2000
Qinghai	36.55	99.60	3196	2	CQPD, 2000

Table 2. Earth's orbital parameters and trace gases as recommended by the PMIP3 project

Simulation	Orbital parameters			Trace gases		
	Eccentricity	Obliquity(°)	Angular precession(°)	CO_2(ppmv)	CH_4(ppbv)	N_2O(ppbv)
PI	0,0167724	23,446	102,04	280	760	270
MH	0,018682	24,105	0,87	280	650	270

Table 3. PMIP3 model characteristics and references

Model Name	*Modelling centre*	*Type*	*Grid*	*Reference*
BCC-CSM-1-1	BCC-CMA (China)	AOVGCM	Atm: 128×64×L26; Ocean: 360×232×L40	Xin et al. (2013)
CCSM4	NCAR (USA)	AOGCM	Atm: 288 × 192×L26; Ocean: 320×384×L60	Gent et al. (2011)
CNRM-CM5	CNRM&CERFACS (France)	AOGCM	Atm: 256 × 128×L31; Ocean: 362×292×L42	Voldoire et al. (2012)
CSIRO-Mk3-6-0	QCCCE, Australia	AOGCM	Atm: 192 × 96×L18; Ocean: 192×192×L31	Jeffrey et al. (2013)
FGOALS-g2	LASG-IAP (China)	AOVGCM	Atm: 128 × 60×L26; Ocean: 360×180×L30	Li et al. (2013)
FGOALS-s2	LASG-IAP (China)	AOVGCM	Atm: 128 × 108×L26; Ocean: 360×180×L30	Bao et al. (2013)
GISS-E2-R	GISS (USA)	AOGCM	Atm: 144 × 90×L40; Ocean: 288×180×L32	Schmidt et al. (2014a,b)
HadGEM2-CC	Hadley Centre (UK)	AOVGCM	Atm: 192 × 145×L60; Ocean: 360×216×L40	Collins et al. (2011)
HadGEM2-ES	Hadley Centre (UK)	AOVGCM	Atm: 192 × 145×L38; Ocean: 360×216×L40	Collins et al. (2011)
IPSL-CM5A-LR	IPSL (France)	AOVGCM	Atm: 96 × 96×L39; Ocean: 182×149×L31	Dufresne et al. (2013)
MIROC-ESM	Utokyo&NIES (Japan)	AOVGCM	Atm: 128×64×L80; Ocean: 256×192×L44	Watanabe et al. (2011)
MPI-ESM-P	MPI (Germany)	AOGCM	Atm: 196×98×L47; Ocean: 256×220×L40	Giorgetta et al. (2013)
MRI-CGCM3	MRI (Japan)	AOGCM	Atm: 320 × 160×L48; Ocean: 364×368×L51	Yukimoto et al. (2012)

Clim. Past Discuss., https://doi.org/10.5194/cp-2018-145
Manuscript under review for journal Clim. Past
Discussion started: 13 November 2018

Table 4. Importance values for each plant life form used in the ΔV statistical calculation as assigned to the megabiomes

Megabiomes	*Life form*		
	Trees	**Grass/grass**	**Bare ground**
Tropical forest	1		
Warm mixed forest	1		
Temperate forest	1		
Boreal forest	1		
Grassland and dry shrubland	0,25	0,75	
Savanna and dry woodland	0,5	0,5	
Desert		0,25	0,75
Tundra		0,75	0,25

Table 5. Attribute values and the weights for plant life forms used by the ΔV statistic

Life form	*Attribute*			
Trees	Evergreen	Needle-leaf	Tropical	Boreal
Tropical forest	1	0	1	0
Warm mixed forest	0,75	0,25	0	0
Temperate forest	0,5	0,5	0	0,5
Boreal forest	0,25	0,75	0	1
Grassland and dry shrubland	0,75	0,25	0,75	0
Savanna and dry woodland	0,25	0,75	0	0,5
weights	0,2	0,2	0,3	0,3
Grass/Shrub	Warm	Arctic/alpine		
Grassland and dry shrubland	1	0		
Savanna and dry woodland	0,75	0		
Desert	1	0		
Tundra	0	1		
weights	0,5	0,5		
Bare Ground	Arctic/alpine			
Desert	0			
Tundra	1			
weight	1			

Table 6. Regression coefficients between the reconstructed climates by inverse vegetation models and observed meteorological values

Climate parameter	Slope	Intercept	R	ME	RMSE
MAT	0,82±0,02	0,92±0,18	0,89	0,16	3,25
MTCO	0,81±0,01	-1.79±0,18	0,95	-0.17	3,19
MTWA	0,75±0,03	4,57±0,60	0,75	-0,19	4,02
MAP	1,15±0,02	32,90±18,41	0,94	138,01	263,88
Pjan	1,01±0,02	0,32±0,47	0,94	0,52	8,89
Pjul	1,30±0,03	-21,67±4,52	0,89	16,45	52,9

The climatic parameters used for regression are the actual values. MAT annual mean temperature, MTCO mean temperature of the coldest month, MTWA mean temperature of the coldest month, MAP annual precipitation, RMSE the root-mean-square error of the residuals, ME mean error of the residuals, Pjan: precipitation of January, Pjul: precipitation of July, R is the correlation coefficient, ± stand error

Clim. Past Discuss., https://doi.org/10.5194/cp-2018-145
Manuscript under review for journal Clim. Past
Discussion started: 13 November 2018

Climate of the Past Discussions
Open Access
EGU

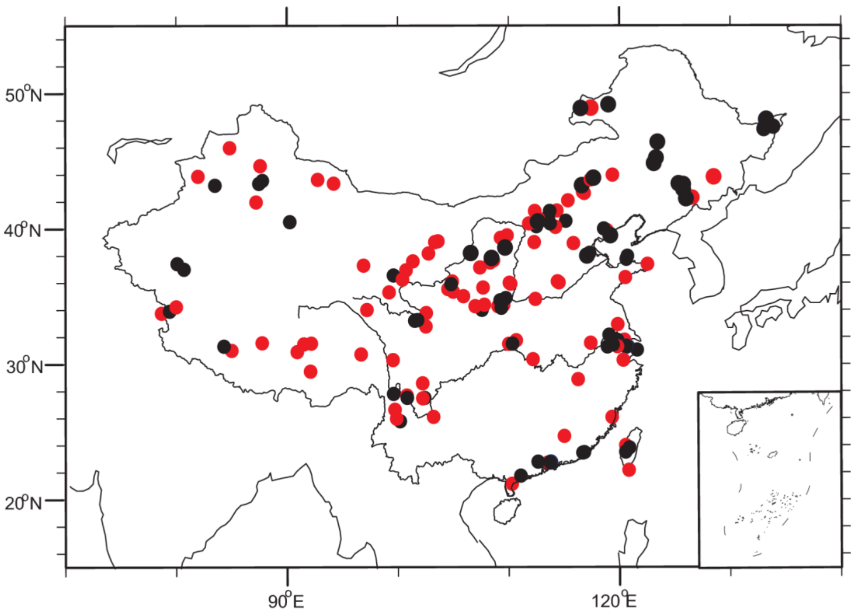

Figure 1. Distribution of pollen sites during mid-Holocene period in China. Black circle is the original China Quaternary Pollen Database and the red circles are new-added ones in this study.

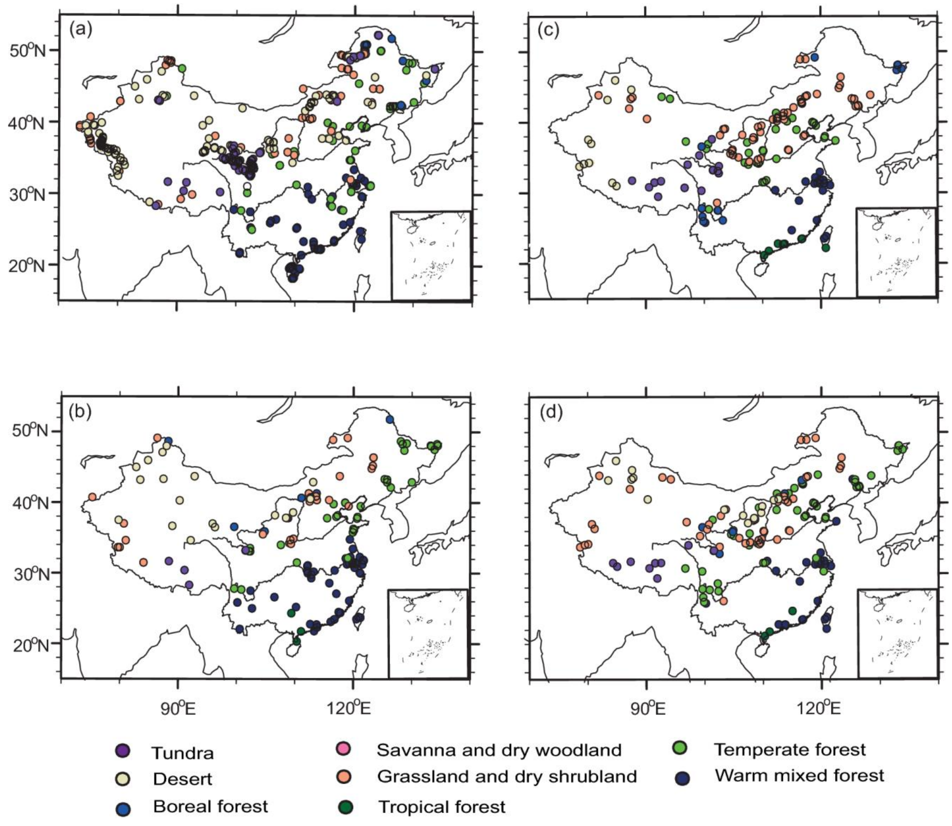

Figure 2. Comparison of megabiomes for PI (first row) and MH (second row): (a,b) BIOME6000, (c,d) pollen data collected in this study.

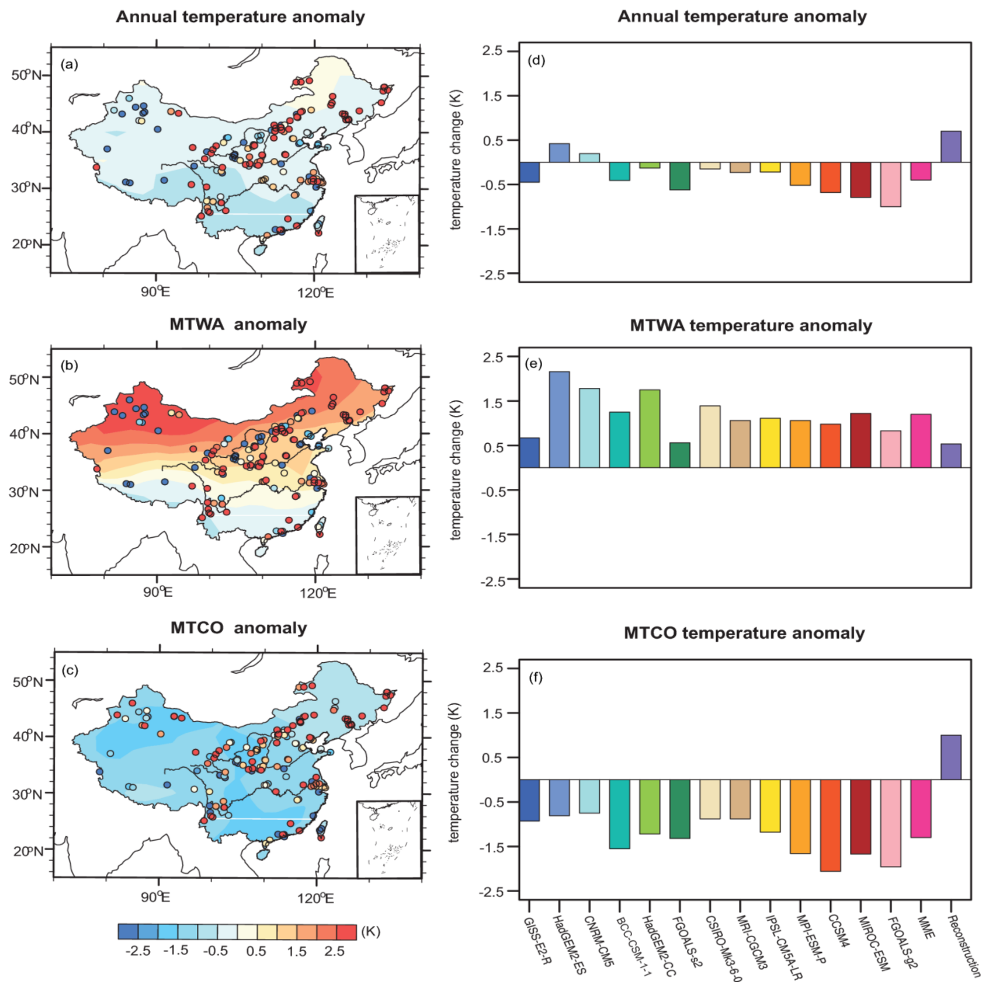

Figure 3. Model-data comparison for annual and seasonal (MTWA and MTCO) temperature (K). For the left panel (a-c), points represent the reconstruction from IVM, shads show the last 30-year means simulation results of multi-model ensemble (MME) for 13 PMIP3 models. The grid mean value of temperature for each model, MME and reconstruction are also displayed at the right panel (d-f).

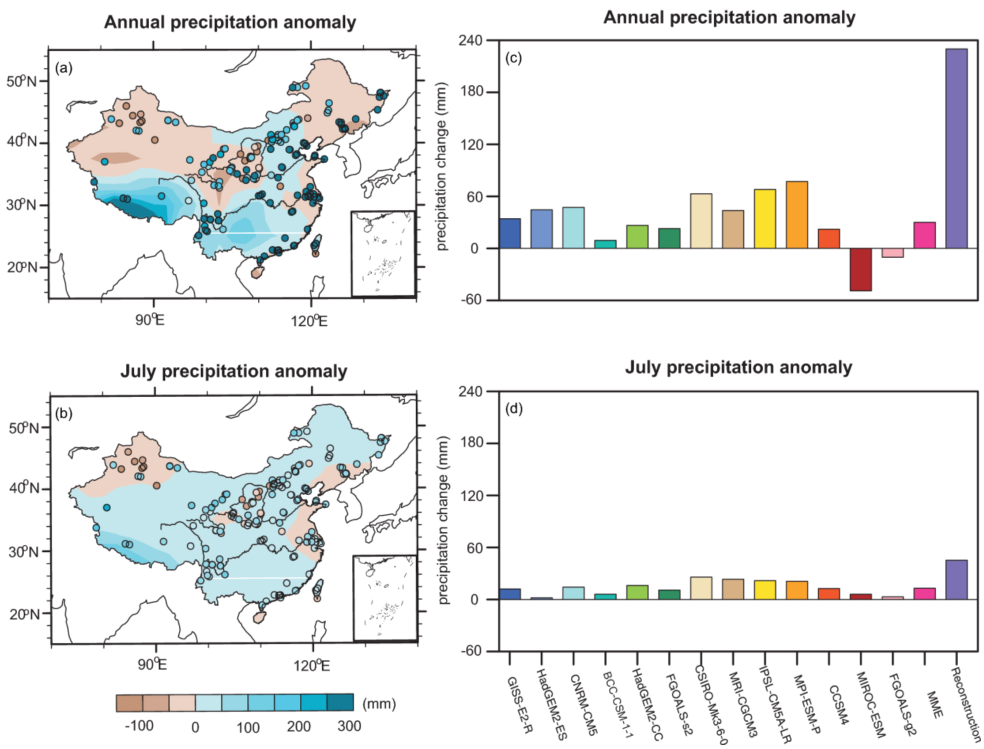

Figure 4. Model-data comparison for annual and July precipitation (mm). For the left panel (a,b), points represent the reconstruction from IVM, shads show the last 30-year means simulation results of multi-model ensemble (MME) for 13 PMIP3 models. The grid mean value of precipitation for each model, MME and reconstruction are also displayed at the right panel (c,d).

Clim. Past Discuss., https://doi.org/10.5194/cp-2018-145
Manuscript under review for journal Clim. Past
Discussion started: 13 November 2018

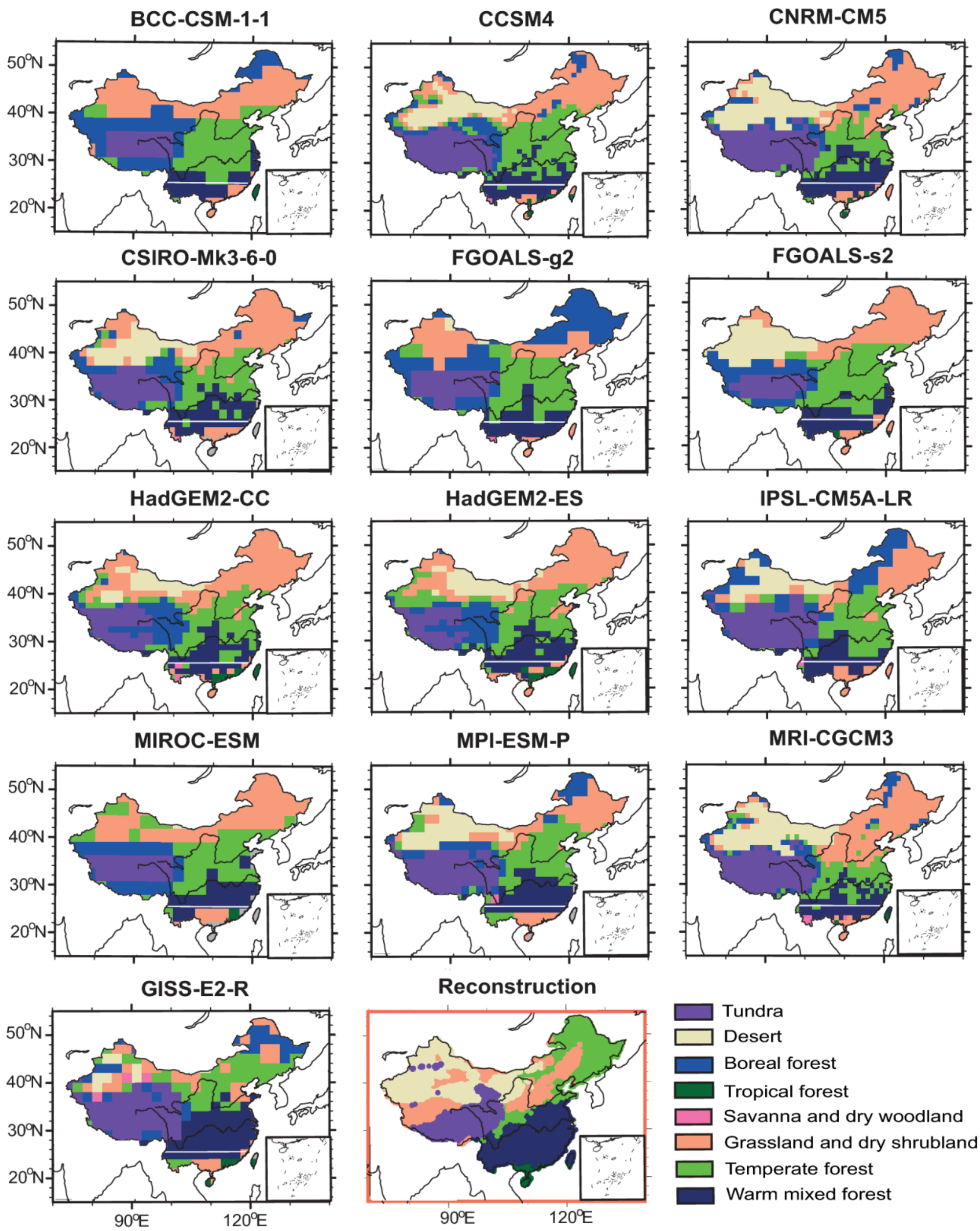

Figure 5. Comparison of interpolated megabiomes distribution (plot in red rectangle) with the simulated spatial pattern from BIOME4 for each model during mid-Holocene.

Clim. Past Discuss., https://doi.org/10.5194/cp-2018-145
Manuscript under review for journal Clim. Past
Discussion started: 13 November 2018

Climate of the Past Discussions
Open Access
EGU

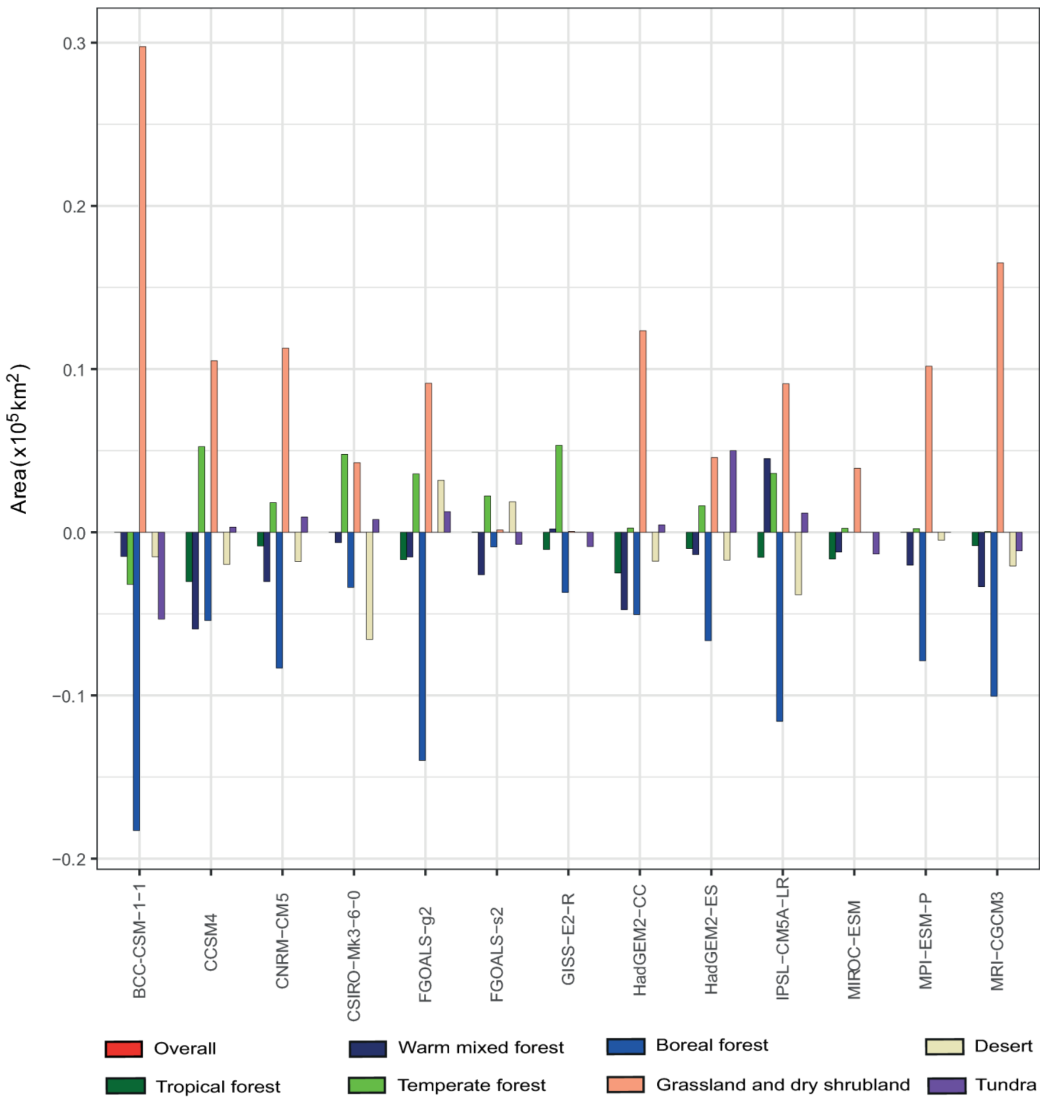

Figure 6. Changes in the extent of each megabiome as a consequence of simulated climate changes for each model, both expressed as change relative to the PI extent of same megabiome. (TrFo: Tropical forest, WaMxFo: Warm mixed forest, TeFo: Temperate forest, BoFo: Boreal forest, Gra/Sh: Grassland and dry shrubland, Sav/Wo: Savanna and dry woodland, Desert: Desert, Tund: Tundra)

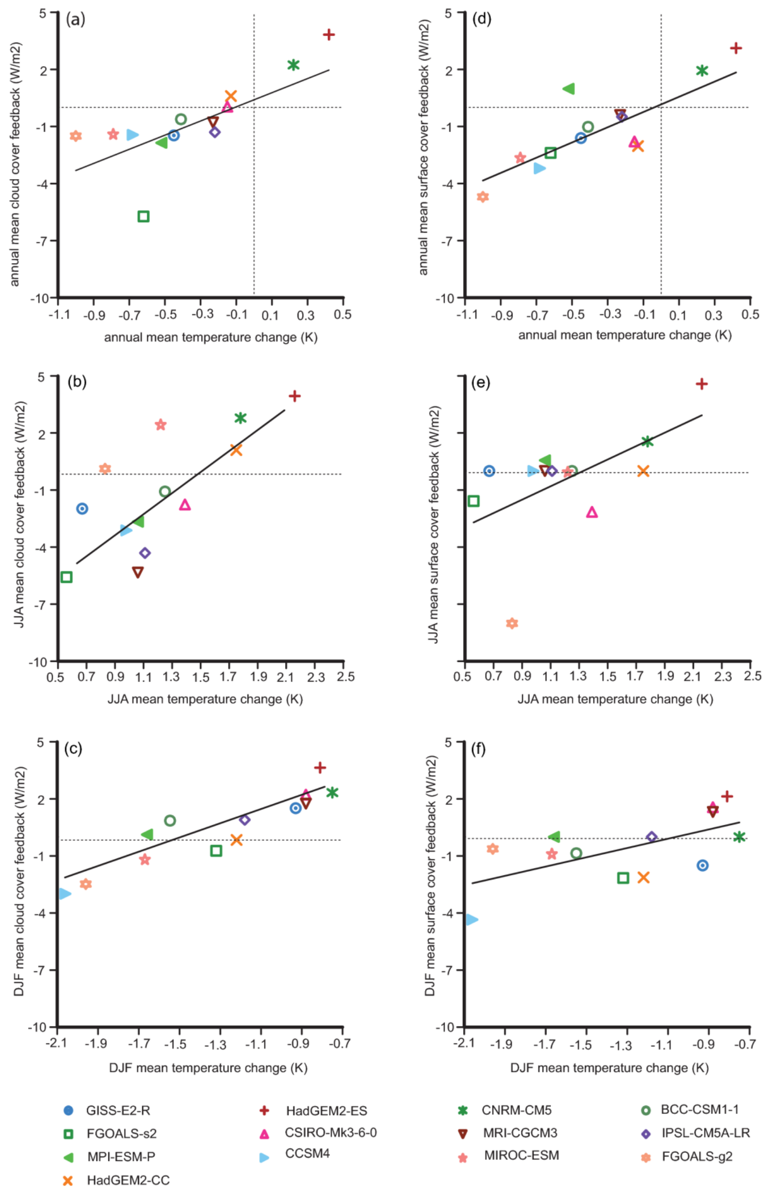

Figure 7. Scatter plots showing temperature, cloud cover feedback and surface albedo feedback changes during MH. The values shown are the simulated 30-year mean anomaly (MH-PI) for the 13 models. **a**, annual mean temperature relative to the annual mean cloud cover feedback and d, annual surface albedo feedback. b, Summer (JJA) mean temperature relative to the summer mean cloud cover feedback and **e**, Summer surface albedo feedback. **c**, Winter (DJF) mean temperature relative to the summer mean cloud cover feedback and **f**, Winter surface albedo feedback.